Heliyon 10 (2024) e26048

Contents lists available at ScienceDirect

Heliyon

journal homepage: www.cell.com/heliyon

Research article

Computational, optical and feasibility studies of organic luminescence TMB-PPT blend for photovoltaic application

Tejas Sharma [a], Thi Thu Ha Nguyen [b], Ngoc Ha Nguyen [b], Hoang Lan Ngo [b], Yew Hang Soo [a], Chai Yan Ng [a,c], H.K. Jun [a,c,d,*]

[a] *Department of Mechanical and Materials Engineering, Lee Kong Chian Faculty of Engineering and Science, Universiti Tunku Abdul Rahman, Sungai Long Campus, Jalan Sungai Long, Bandar Sungai Long, 43000 Kajang, Malaysia*
[b] *Department of Theoretical and Physical Chemistry, Faculty of Chemistry, Hanoi National University of Education, 136 Xuan Thuy, Cau Giay, Hanoi, Viet Nam*
[c] *Centre for Advanced and Sustainable Materials Research, Universiti Tunku Abdul Rahman, Sungai Long Campus, Jalan Sungai Long, Bandar Sungai Long, 43000 Kajang, Malaysia*
[d] *Centre for Sustainable Mobility Technologies, Universiti Tunku Abdul Rahman, Sungai Long Campus, Jalan Sungai Long, Bandar Sungai Long, 43000 Kajang, Malaysia*

ARTICLE INFO

Keywords:
Perovskite solar cell
Long persistent luminescence
After-glow effect

ABSTRACT

For enhanced applications of solar cells, organic luminescence materials like long persistent luminescence (LPL) present one of the promising avenues for light enhancement. Currently, most existing luminescent materials are based on an inorganic system that requires rare elements such as europium and dysprosium, with a very high processing temperature. Adopting organic luminescence materials that are free from rare elements is necessary, considering the low-temperature fabrication and low material cost. In this work, we investigate the optical properties of an organic luminescence blend consisting of 2,8-bis(diphenylphosphoryl)dibenzo [*b*,*d*]thiophene (PPT) and N,N,N′,N'-tetramethylbenzidine (TMB) through computational studies and experimental validations. Optical characteristics of the luminescence materials like optical absorption, photoluminescence, and time-resolved photoluminescence spectroscopy are characterized. To validate the functionality of the organic luminescence blend, the material is incorporated into the perovskite solar cell structure. Unfortunately, the blend is unable to emit sufficient illumination over extended periods due to its low intersystem crossing efficiency and weak spin-orbit coupling. Although the power conversion efficiency of the Luminescence/FTO/TiO2/Perovskite/Carbon structure is observed to be small under dark conditions, the application of organic luminescence materials can be further enhanced and explored.

1. Introduction

Glow-in-the-dark materials have been the subject of numerous research due to their ability to emit light in the dark after exposure to light. The source of this persistent emission can be attributed to photoluminescence, chemiluminescence, or radioluminescence. Applications of this phenomenon can be found in glow-in-the-dark paints, where radioluminescence is emitted constantly without the

* Corresponding author. Department of Mechanical and Materials Engineering, Lee Kong Chian Faculty of Engineering and Science, Universiti Tunku Abdul Rahman, Sungai Long Campus, Jalan Sungai Long, Bandar Sungai Long, 43000 Kajang, Malaysia.
E-mail addresses: junhk1@gmail.com, junhk@utar.edu.my (H.K. Jun).

https://doi.org/10.1016/j.heliyon.2024.e26048
Received 21 December 2023; Received in revised form 6 February 2024; Accepted 7 February 2024
Available online 8 February 2024

need for photoexcitation. However, due to the presence of radioactive elements, radioluminescence materials have been gradually replaced by long persistent luminescence (LPL) materials, which rely on the photoluminescence effect for their mechanism. LPL, also known as long persistent phosphorescence or long-lasting afterglow/phosphorescence, plays a crucial role in various fields including spectroscopy, photochemistry, photonics, and materials research, owing to its unique process of storing and releasing photoelectrons. High-performance LPL materials gained significant traction and were extensively applied in watches and emergency lights in the mid-1990s [1]. They continue to pique the curiosity of materials scientists, chemists, physicists, and even biologists due to the intriguing optical phenomena and the wide range of applications they offer. LPL materials have the capacity to retain and gradually release the absorbed energy, resulting in a long-lasting visible emission. This stands in contrast to conventional phosphorescent or fluorescent materials, which produce light for only a brief period of time following light stimulation [2–4].

LPL materials are categorized into two groups: inorganic LPL and organic LPL, depending on their structure and chemistry. Examples of host materials frequently used to fabricate inorganic LPL include strontium aluminate ($SrAl_2O_4$) and zinc sulfide (ZnS). These materials commonly exhibit strong and long-lasting luminescence phenomena due to the presence of deep trap states and efficient energy transfer mechanisms. However, the synthesis methods of inorganic LPL are inflexible and often require high manufacturing temperatures, especially when the LPL host is dispersed in polymer media for large-scale applications [2]. On the other hand, organic LPL materials can exhibit persistent luminescence through processes such as triplet-triplet annihilation, delayed fluorescence, or thermally induced delayed fluorescence. Moreover, compared to inorganic LPL materials, they offer advantages in adaptability, solution processability, and tunable emission colors [5].

The majority of organic photoluminescent compounds with persistent emissions are derived from phosphorescent substances. Although competing nonradiative processes frequently extinguish phosphorescence, various organic systems with long-lasting phosphorescence at ambient temperature have been discovered [5–8]. In early years, the first organic molecules reported to exhibit photo-ionization resulted from two-photo absorption [9]. However, this photoionization process requires strong excitation power. To address this, Kabe and Adachi recently synthesized an alternative organic LPL system exhibiting one-photon ionization by combining the electron donors from 2,8-bis(diphenylphosphoryl)dibenzo [*b*,*d*]thiophene (PPT) with N,N,N′,N’-tetramethylbenzidine (TMB) via the melt casting method (see Fig. 1 for their molecular structures) [10].

LPL materials have attracted particular interest as potential materials to increase photovoltaic (PV) device efficiency. It is well-known that a PV cell can only produce electricity when there is a light source, typically during the daytime. Combining photovoltaic cells with LPL materials can address this issue by enabling emission even in a dark environment. After being excited by a light source, persistent luminescence materials can store energy and continue to emit light over time. This technique is especially beneficial in low-light situations, as it can enhance the performance and efficiency of the cells. Additionally, to achieve the required spectrum conversion, LPL materials can be designed to absorb light intensity in a particular spectral region and re-emit it in another [11]. By matching the spectral response of the photovoltaic material to the absorption spectrum of the solar cell, this approach may be utilized to improve the solar cell’s absorption spectrum and increase the efficiency of the cell [12]. Furthermore, LPL materials can also be used for light management and concentration in PV cells. They can reroute and convert specific wavelengths of light to match the absorption properties of the solar cell material, using luminescent up-conversion or down-conversion processes [13]. In this work, the optical properties of organic luminescence materials consisting of a blend of TMB and PPT were simulated to assess the feasibility of integrating these materials into perovskite solar cell applications. Subsequently, the experimental validation of this organic luminescence material blend was conducted to demonstrate its application feasibility. It is theorized that the TMB-PPT blend can function as LPL materials, as demonstrated under controlled environments [10]. However, their practicality under ambient conditions for solar cell applications has yet to be reported. Therefore, this study aims to investigate whether the organic luminescence blend can serve as a secondary light source, especially under dark conditions, for photovoltaic applications.

2. Experimental

2.1. Computational methods

Structural optimization calculations were first performed, followed by the utilization of the linear-response time-dependent density functional theory (LR-TDDFT) method to calculate the UV-VIS and PL spectra of TMB, PPT, and the TMB:PPT mixture at ratios of 1:1 (T1P1) and 2:1 (T2P1). The PBE0/DZVP basis set was employed with a cut-off energy of 350 Ry in the calculations, which were performed using the open-source software CP2K [14].

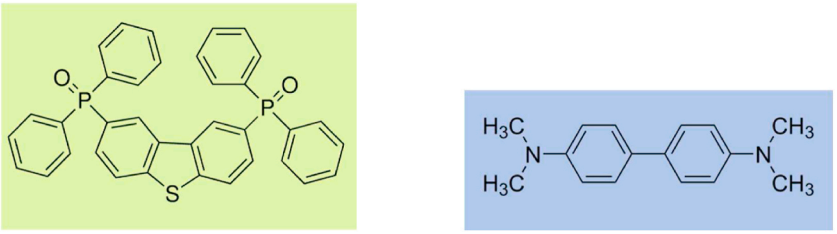

Fig. 1. Structure of PPT (left) and TMB (right).

2.2. Preparation of organic luminescence blend samples and characterization

N,N,N′,N'-tetramethylbenzidine (TMB) and 2,8-bis(diphenylphosphoryl)dibenzo [*b*,*d*]thiophene (PPT) were used as supplied by Sigma-Aldrich. For film fabrication, the traditional melt-casting technique was employed. A mixture of TMB and PPT (totaling 100 mg) was placed on a glass substrate for 10 s in the open air, then heated to 250 °C. After melting, the substrate was quickly cooled to room temperature and enclosed in glass coverings made of ultraviolet-cured epoxy resin under ambient conditions. Various samples were prepared by varying the ratio of TMB and PPT, as shown in Table 1.

2.3. Fabrication and characterization of perovskite solar cell samples

A compact electron transport layer (ETL) was deposited by spin-coating a TiO_2 solution on the conducting glass substrate at 3000 rpm for 30 s followed by annealing at 450 °C. Subsequently, a mesoporous TiO_2 layer was applied on top of the compact TiO_2 layer by spin-coating a solution of TiO_2 paste diluted in ethanol (1:3.5 mass ratio) at 5000 rpm for 30 s, followed by annealing at 450 °C for 30 min.

For the perovskite active layer, 50 μL of $FAMAPbI_3$ solution was deposited on the mesoporous TiO_2 layer using a one-step spin-coating method at room temperature. To achieve a reflective and shiny surface of the perovskite layer, vacuum-flash assisted solution processing (VASP) treatment was applied as an anti-solvent method. In this process, the sample was placed in a sample chamber attached to a laboratory-made vacuum pumping instrument. By opening the valve connecting the specimen chamber and the pump system, the perovskite film was subjected to low pressure sustained at 20 Pa for 10 s. Full re-pressurization then occurred by allowing ambient air to enter the specimen chamber [15]. Finally, isostatic pressing was applied to the sample. The solar cell sample preparation is briefly illustrated in Fig. 2(a–f), and its schematic structure is shown in Fig. 2(g).

Organic luminescence samples were experimentally validated through characterization in UV–Vis absorption, photoluminescence (PL) response, and time-resolved photoluminescence (TRPL). Meanwhile, the perovskite solar cell samples were tested with and without a luminescence materials layer under light and dark conditions. For comparison, an inorganic luminescence material of $SrAl_2O_4$ was also tested with the solar cell samples.

3. Results and discussion

3.1. Computational studies

The calculated spectra are presented in Figs. 3 and 4. In Tables 2 and 3, we provide a comparison of the HOMO-LUMO gap and excitation energy in the UV-VIS and PL spectra of pure TMP (Figs. 3(a) and 4a) and PPT (Figs. 3(b) and 4b), as well as T1P1 (Figs. 3(c) and 4c) and T2P1 (Figs. 3(d) and 4d). The comparison of oscillator strength values reveals that PPT exhibits a better light absorption capability than TMB. The results obtained indicate a decrease in the light absorption capacity of the mixture compared to each pure substance. The TMB:PPT mixture in a 1:1 ratio showed light absorption in the visible region. When the TMB ratio was doubled in the TMB:PPT mixture (2:1), the maximum absorption peak shifted towards the infrared region. This shift in the maximum absorption peak towards the infrared region in the TMB:PPT mixture with a ratio of 2:1 can be explained by the change in the electronic properties of the mixture.

Fig. 5(a-b) depicts the HOMO and LUMO images of the T1P1 and T2P1 mixtures. It can be observed that the HOMO is mainly contributed by TMB, while the LUMO of the system is contributed by PPT. In both mixtures, upon photon excitation, the HOMO (TMB) → LUMO (PPT) transition occurs.

The computed interaction energy values for the TMB + PPT → T1P1 and 2TMB + PPT → T2P1 processes were found to be positive, with values of 171.29 kJ/mol and 267.75 kJ/mol, respectively. This implies that TMB and PPT do not form a composite but rather exist as a mixture where there is no interaction between the two. As a result, the TMB and PPT system can be regarded as a heterojunction system, and the electron transition process can occur as illustrated in Fig. 6.

The shift of the maximum absorption peak towards longer wavelengths in the TMB:PPT mixture, compared to pure TMB and PPT, can be attributed to the electron transition from the HOMO of TMB to the LUMO of PPT, which requires less energy than transitions from HOMO (TMB) to LUMO (TMB) or from HOMO (PPT) to LUMO (PPT).

Table 1
Composition of TMB and PPT for Cell-1 to 5.

Sample	Mass ratio TMB:PPT	Mass of TMB (mg)	Mass of PPT (mg)
Pure TMB	1:0	50	0
Pure PPT	0:1	0	50
Cell-1	1:1	50	50
Cell-2	3:2	60	40
Cell-3	7:3	70	30
Cell-4	4:1	80	20
Cell-5	9:1	90	10

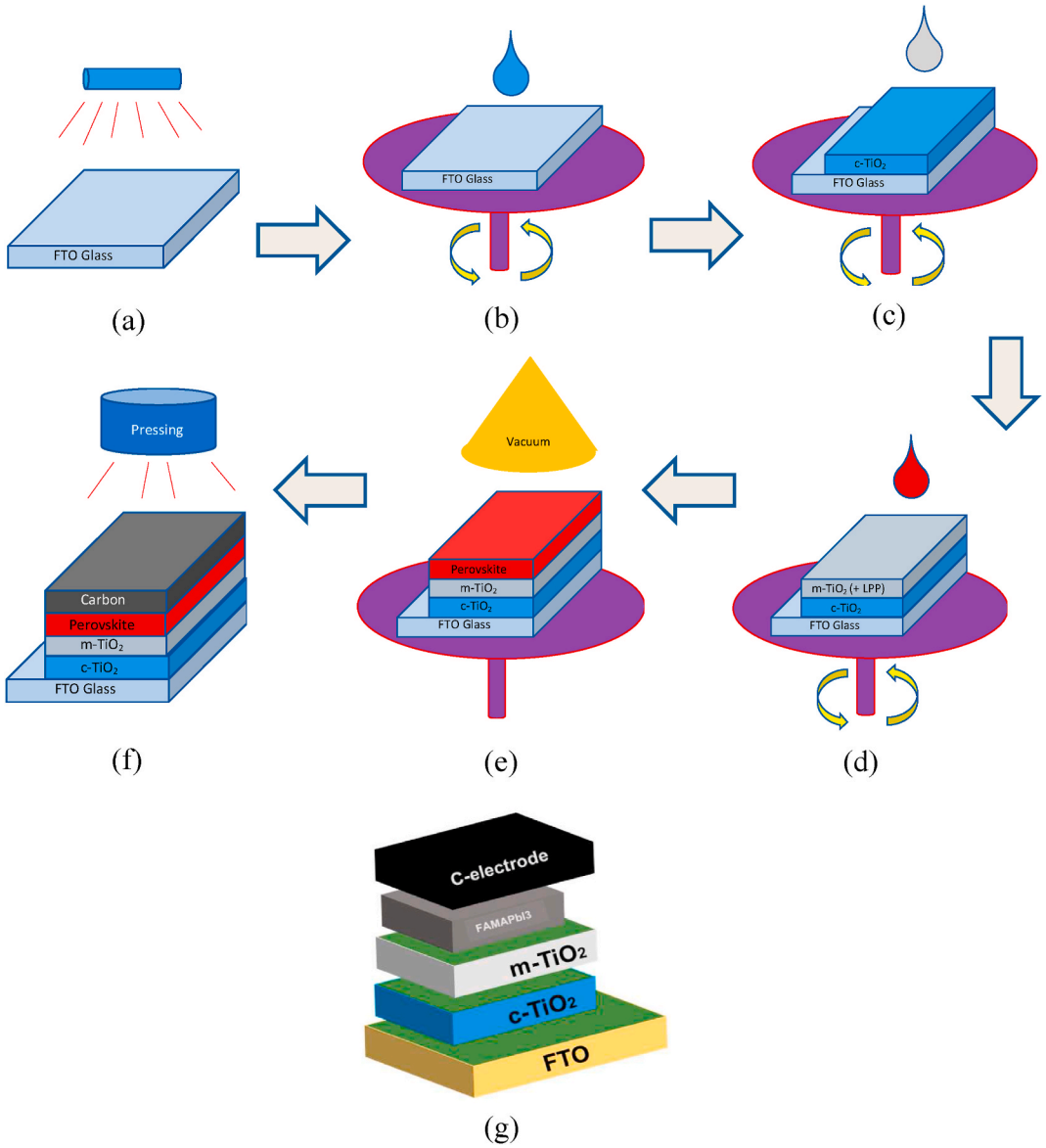

Fig. 2. Fabrication flow of the perovskite solar cell samples: (a) Substrate cleaning by UV light, (b) spin-coating compact TiO_2 layer, (c) spin-coating mesoporous TiO_2 layer, (d) spin-coating perovskite layer, (e) vacuum flash-assisted process, and (f) isostatic pressing of the sample, and (g) schematic of the PSC structure.

3.2. Optical characterization

3.2.1. UV-VIS spectra

The UV–Vis absorbance spectra provide crucial details about a material's ability to absorb light in the ultraviolet (UV) and visible portions of the electromagnetic spectrum. Based on these findings, we can assess the absorbance for the mixture of TMB and PPT, with a combined UV–Vis spectrum ranging from 200 nm to 800 nm. The absorbance spectra are plotted for seven blends, including pure TMB and pure PPT, where Cell-1 to Cell-5 represent mixtures of TMB and PPT. Fig. 7(a) displays the ultraviolet/visible absorption of the samples. From the graph, the absorbance intensity increases as the concentration of PPT increases, and it's evident that Cell-3 (TMB:PPT = 7:3 by mass) has the maximum absorbance value at a wavelength of 350 nm. The peak of Cell-3 indicates that the material absorbs light most strongly at 350 nm. This peak absorbance corresponds to specific molecular or electronic transitions occurring within the substance. The results also corroborate with the simulation, showing absorption activities in the visible region around 350 nm.

Due to their short π-conjugation, both pure TMB and PPT samples also exhibit absorption around 350 nm. The fluorescence maxima of TMB and PPT were located at 394 nm and 346 nm, respectively. We utilized the strong electron-donating compound TMB, which has

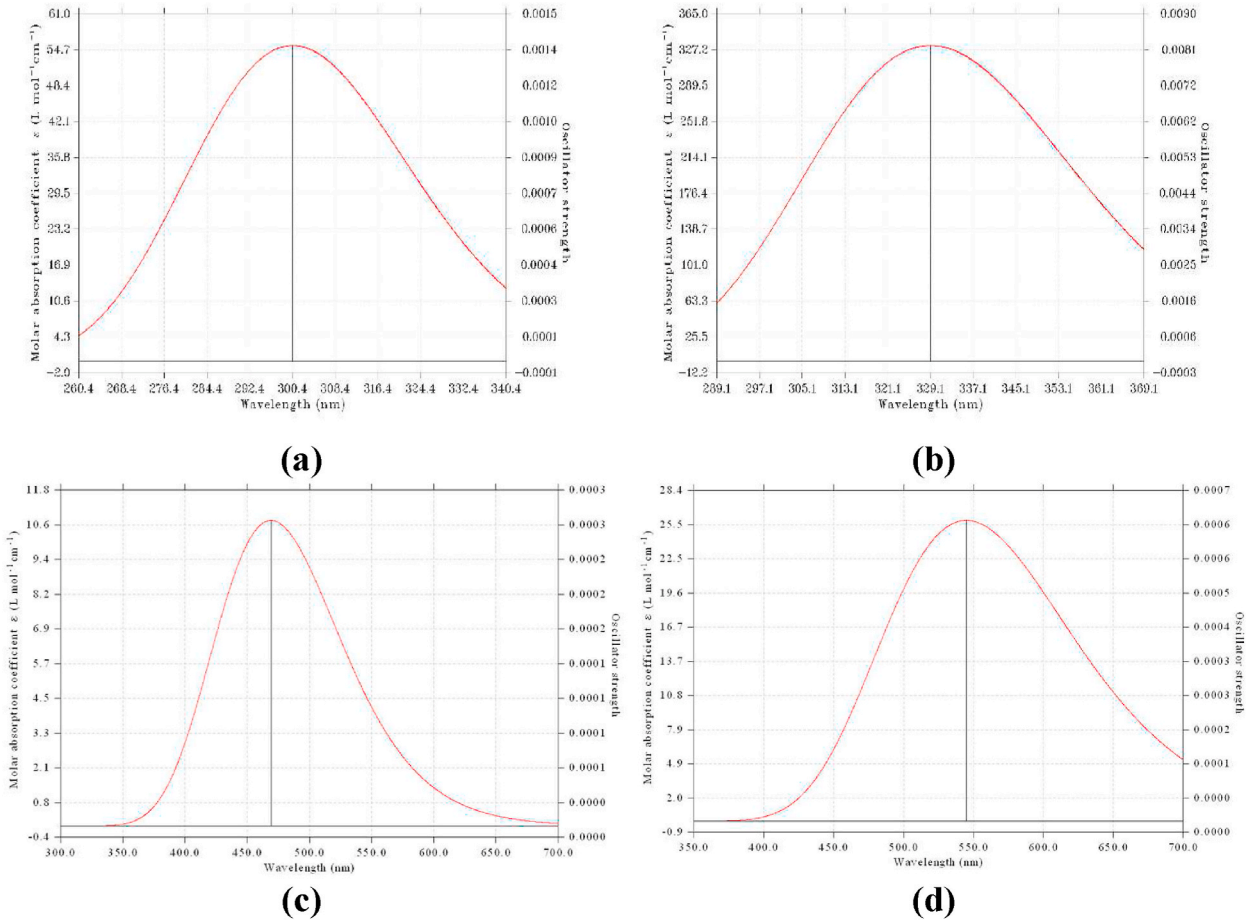

Fig. 3. Calculated UV-VIS spectra for (a) TMP, (b) PPT, (c) T1P1 and (d) T2P1.

an extremely stable radical cation, and the strong electron-accepting molecule to achieve long-lived charge-separated states [6]. If the temperature rises, it will lead to TMB oxidation, in which the maximum absorbance will be altered. The photo-generated radical cations and anions must accumulate in the mixture without losing their energy through recombination. This stands in contrast to organic photovoltaics, where charges are typically swept out of the device.

3.2.2. Photoluminescence (PL) spectra

It is also essential to analyze the specific PL properties of the TMB-PPT mixture. Emission wavelengths and intensities can be influenced by various factors, including the concentrations of TMB and PPT, the local environment, and any interactions between the two materials. In this work, different concentrations of TMB and PPT blends were prepared to study the emission properties of the luminescence materials. When TMB and PPT are mixed together and excited at 350 nm, PL spectra are clearly observed as a result of the electronic transitions taking place in both substances (Fig. 7(b)). TMB, being an organic substance, is well-known for its strong electron-donating abilities. Its structure allows the molecule to transfer charges effectively, facilitating efficient charge transport within the substance.

When TMB absorbs photons at 350 nm, electrons in the molecule are excited to higher energy states. These excited electrons can then recombine with electron holes, releasing energy in the form of light. Similarly, when PPT absorbs photons at 350 nm, it undergoes electronic transitions, and the excited electrons can also recombine with electron holes, resulting in the emission of light [16]. The specific emission characteristics of each component, as well as any potential interactions or energy transfer processes between them, will determine the combined PL spectrum of the TMB and PPT mixture. As a result, the spectrum of pure TMB, pure PPT, and Cell-1 to Cell-5 shows the highest peaks associated with the emission from TMB and PPT around 550 nm. This extended absorption might result from the charge-transfer absorption band or from the presence of a small amount of TMB radical cations, which would absorb in the longer-wavelength regions. Additionally, the duration of luminescence also depends strongly on the doping concentration of TMB. When the concentration of TMB was increased, the emission spectra shifted slightly from 556 nm to 577 nm [17]. However, the peak shifts are not linearly red-shifted. With the pure TMB sample, the maximum peak observed is at 558 nm (see Fig. 7(c)). Upon the addition of PPT in the ratio, the peak shifted to 556 nm for Cell-1. However, as the ratio of TMB increases, the spectra are red-shifted to 571 nm for Cell-2 before blue-shifting to 551 nm for Cell-3. With even higher TMB content, the maximum peaks observed in Cell-4 and

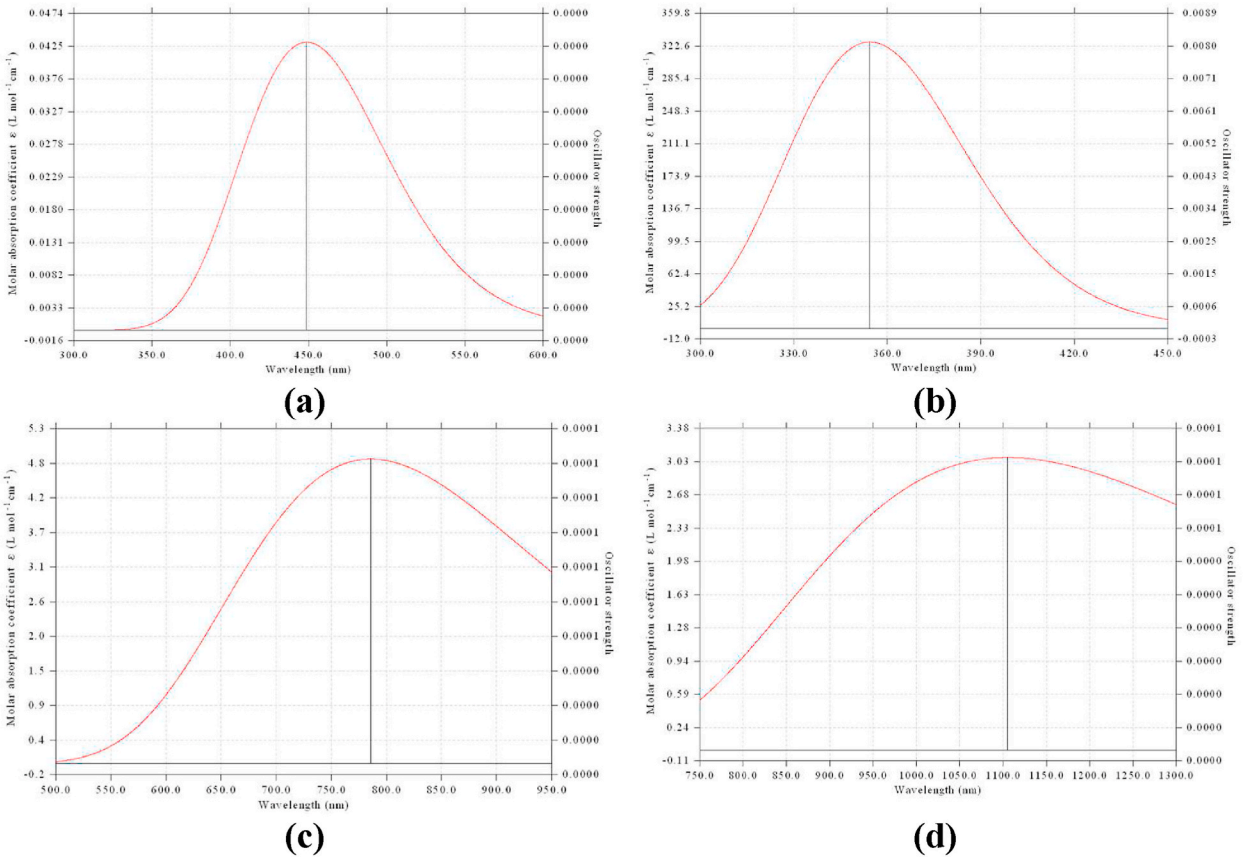

Fig. 4. Calculated PL spectra for (a) TMP, (b) PPT, (c) T1P1 and (d) T2P1.

Table 2
Comparison of HOMO-LUMO gap and excitation energy in UV-VIS and PL spectra of pure TMB and PPT.

	HOMO-LUMO gap (eV)	Excitation Energy (S0, eV)/Oscil.str. (Peak in UV–Vis)	Excitation Energy (S1, eV)/Oscil.str. (Peak in PL)
TMB	4.98	$4.13/1.4 \times 10^{-3}$	2.76/less than 10^{-5}
PPT	4.37	$3.77/8.2 \times 10^{-3}$	$3.50/8.1 \times 10^{-3}$

Table 3
Comparison of HOMO-LUMO gap and excitation energy in UV-VIS and PL spectra of TMP: PPT mixture at ratios of 1:1 and 2:1.

Ratio	HOMO-LUMO gap (eV)	Excitation Energy (S0, eV)/Oscil.str. (Peak in UV–Vis)	Excitation Energy (S1, eV)/Oscil.str. (Peak in PL)
1:1	3.21	$2.64/2.7 \times 10^{-4}$	$1.58/1.2 \times 10^{-4}$
2:1	3.22	$2.28/6.4 \times 10^{-4}$	$1.12/8.0 \times 10^{-5}$

5 are 566 nm and 577 nm, respectively.

In terms of PL quantum yield, the optimum Cell-3 exhibited a quantum yield of 107%, compared to that of pure TMB and pure PPT at 31% and 11%, respectively. The PL quantum yield for Cell-3 is also better than that of Cell-1 and Cell-2, where both exhibited yield values of 37% and 35%, respectively. With lower PPT ratio content, sample Cell-4 produced a lower quantum yield at 54%. As expected, Cell-5 with the lowest PPT ratio content showed an even lower quantum yield at 6%. We opined that the decrease in quantum yield is attributed to insufficient paths for electron transition from PPT to TMB molecules, where a sufficient amount of guest-host molecules is paramount for PL emission.

Nevertheless, the experimental results corroborate with the simulation, where the PL responses are manifested near 700 nm. Specifically, Cell-3 exhibits the highest PL intensity among the samples. The illumination observed in this region matches with the light absorption spectra of the studied perovskite compound.

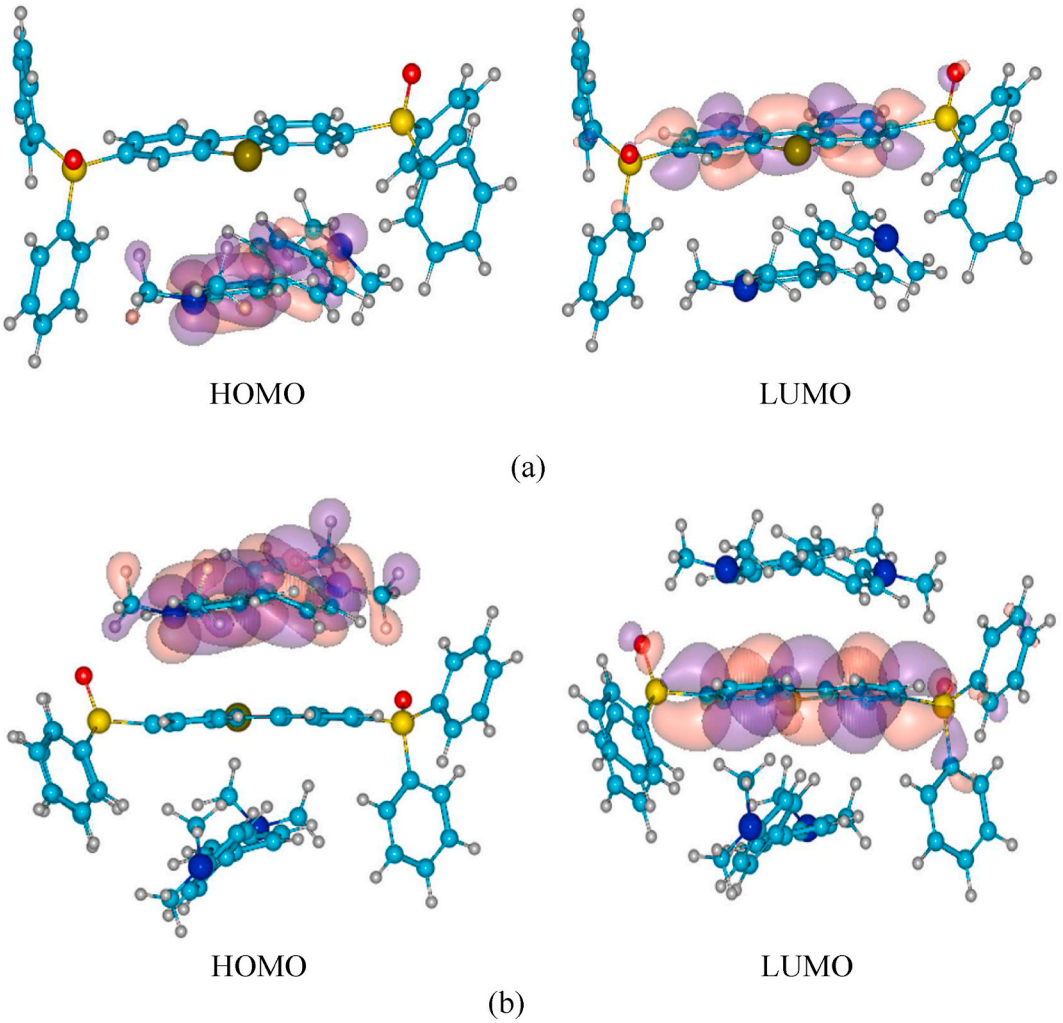

Fig. 5. (a) HOMO, LUMO of T1P1 mixture; (b) HOMO, LUMO of T2P1 mixture.

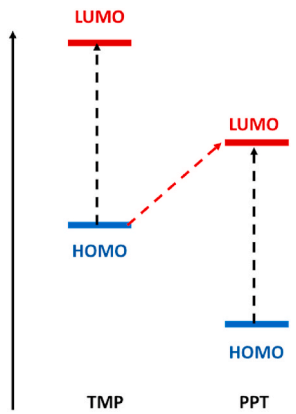

Fig. 6. HOMO and LUMO alignment of TMB-PPT mixture.

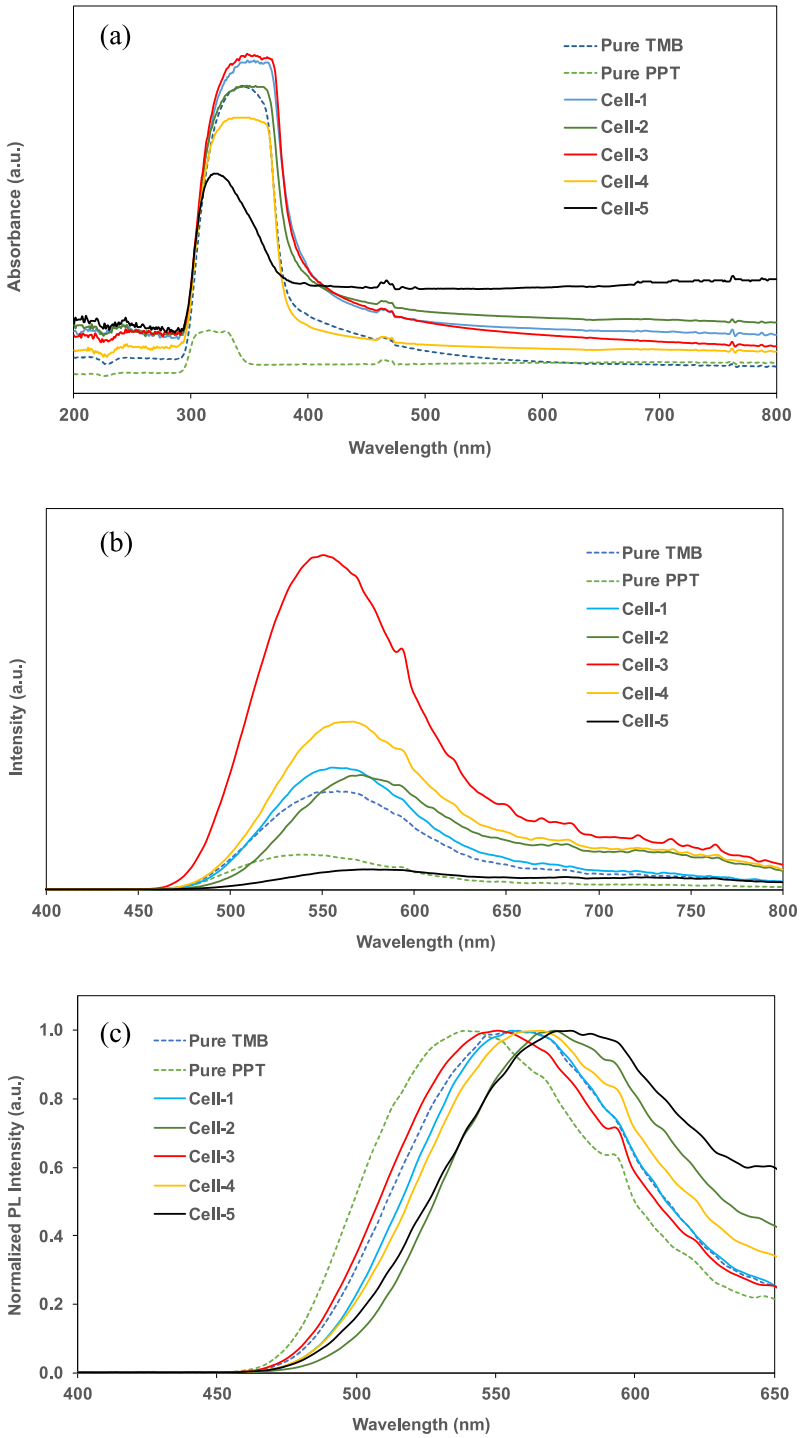

Fig. 7. Spectra of organic luminescence spectra with different ratio of TMB and PPT in (a) UV-VIS; (b) PL; and (c) closed up of normalized PL.

3.3. Luminescence lifetime

Time-resolved photoluminescence (TRPL) spectra are used to study the decay dynamics of the organic luminescence materials. When PPT and TMB are combined, TRPL spectra provide crucial information about the carrier dynamics and recombination processes inside the material. Fig. 8 depicts the lifetime and photon counts of every sample. From the results, all samples exhibit almost the same

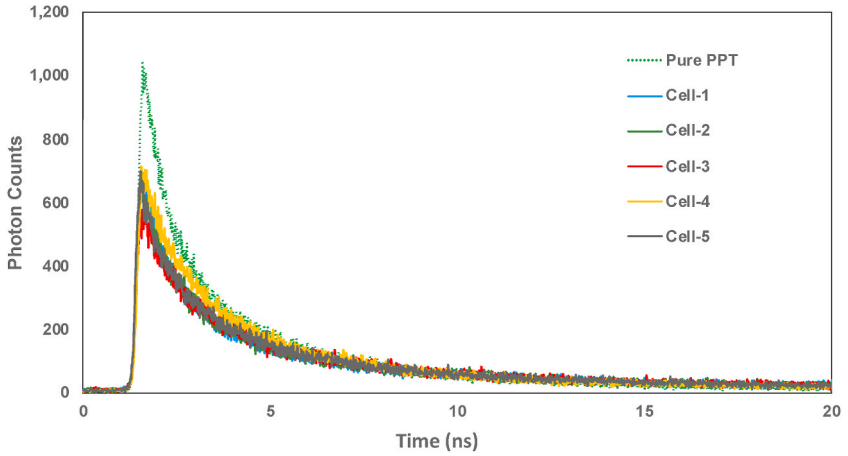

Fig. 8. TRPL of organic luminescence samples.

trend. Cell-3 has the maximum photon counts and longer lifetime among the mixed luminescence blend samples, indicating the decay of electrons at its lowest rate. The analyzed lifetime of Cell-3 shows a higher lifetime compared to that of the pure PPT sample. Consequently, the rate of photon emission from Cell-3 has also increased among the mixed luminescence blend samples, indicating radiative recombination efficiency and the concentration of radiative recombination centers in the material [18]. All the cells showed longer carrier lifetime except for Cell-1 and Cell-2 due to an increase in recombination rates caused by trap states present in blended luminescence.

The lifetime data of the samples were calculated by fitting with the following triple-exponential equation:

$$R(t) = B_1 e^{(-t/\tau_1)} + B_2 e^{(-t/\tau_2)} + B_3 e^{(-t/\tau_3)}$$

where B_1, B_2 and B_3 are amplitude constituent of the first, second and third decay exponents. The decay curve consists of a rapid constituent τ_1 with two slower constituents of τ_2 and τ_3. The average luminescence lifetime of pure PPT is 4.226 ns. When higher ratio of PPT is blended with TMB, as in the case of Cell-1 and Cell-2, the lifetime values are 2.133 ns and 2.110 ns, respectively. The longest lifetime value is observed in Cell-3 with 7.197 ns ($\tau_1 = 0.674$ ns, $\tau_2 = 2.527$ ns, $\tau_3 = 9.997$ ns). Higher ratio of TMB in the blend seems to sustain longer lifetime as manifested in Cell-4 and Cell-5 with lifetime values of 6.020 ns and 7.196 ns, respectively. Due to the short lifetime observed, which is at 7 ns, we expect the luminescence effect of the organic luminescence blend to be short-lived or negligible, which opposes the behavior of LPL materials. It should be noted that the influence of excitation power was not studied in this work. This is because the luminescence blend samples have been tested previously in separate work, with a different excitation mode where it was concluded that only excitation in standard range is sufficient for the luminescence effect study. Furthermore, the application of the samples was only validated under ambient temperature.

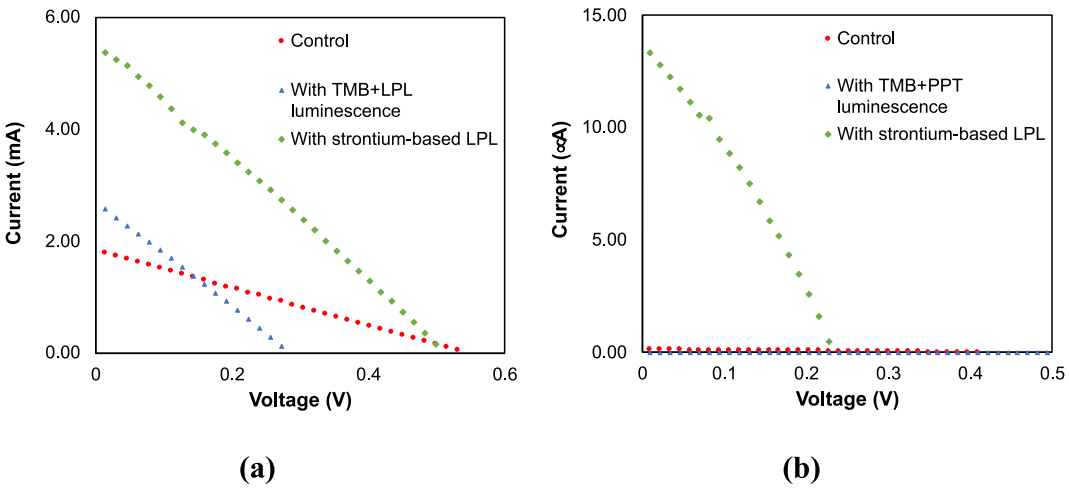

Fig. 9. I–V curves for perovskite solar cells with or without organic luminescence blend, tested under (a) xenon lamp illumination, and (b) dark.

3.4. Feasibility of incorporating luminescence materials to perovskite solar cell

To test the effect of luminescence materials on perovskite solar cell (PSC), luminescence layer was coated on a clear glass substrate. The coated luminescence substrate was then externally coupled with the carbon-based PSC samples, with the luminescence layer on top of the PSC glass substrate. The assembly was tested under xenon lamp illumination with irradiance of 0.8 sun. This was followed by testing under dark conditions after 5 min of light exposure. Fig. 9(a) shows the I–V curves of the assembly tested under light while Fig. 9(b) presents the results under dark conditions. Meanwhile, Table 4 lists the I–V parameters of the samples tested under light and dark conditions.

A control sample demonstrates a low efficiency value under light, with a calculated efficiency of 2.21%, which is lower than those reported elsewhere [19]. We attribute the low performance to internal resistance within the solar cell configuration, and we do not rule out the possibility of partial shorting in the solar cell structure. Therefore, optimization of the configuration is needed, which is the focus of our subsequent study and will be reported in a separate publication. Nevertheless, the control sample shall be used as a benchmark in this study.

When the same control sample was tested under dark conditions (after light soaking for 5 min), no output was detected other than the open-circuit voltage. However, when the similar sample was coupled with an inorganic LPL layer (i.e. strontium-based LPL), the efficiency improved to 6.63%. The enhancement is attributed to the improved current generated i.e. improved light harvesting via a down-converting mechanism [20,21]. When the assembly was tested under dark, after light soaking, a minute amount of output was detected. From visual observation, the inorganic LPL layer demonstrated low illumination due to the self-illumination of the LPL materials. The performance of the assembly under dark conditions is 1.03%, which is better than expected, although the open-circuit voltage decreased.

Unfortunately, when the PSC sample was coupled with an organic luminescence layer (i.e. mixture of TMB-PPT), there was no positive effect derived from the organic luminescence. The efficiency of the assembly decreased to 1.75%, which is lower than the control sample. This reduction in performance is attributed to the light blocking and absorbance of the luminescence layer, reducing the amount of photons reaching the perovskite layer. When the organic luminescence assembly was tested under dark conditions after light soaking, the output was small, with an efficiency recorded at 0.08%. Visually, there was no appreciable self-illumination observed on the organic luminescence layer. The low self-illumination after light soaking could be due to rapid charge recombination upon photo-excitation in the organic luminescence layer. This observation corroborates with the short charge lifetime as calculated in the TRPL analysis (section 3.3). Despite the low performance of the assembly with the organic luminescence layer under dark conditions, there is room for improvement, where optimized encapsulation of the luminescence layer could yield a longer charge lifetime for extended self-illumination in the dark.

4. Conclusions

In this work, organic luminescence blend of TMB and PPT has been studied via computational methods, followed by experimental validation of its optical properties. Computational studies of the TMB and PPT blend have demonstrated the possibility of PL responses in the visible region. Experimental characterization validated that the PL of the blends manifested around peak values between 550 and 570 nm, falling within the absorption range of the perovskite compound. The best blend consists of TMB:PPT in a mass ratio of 7:3, where a high PL quantum yield was observed among the samples. However, when the optimum organic luminescence blend layer was assembled with the perovskite solar cell, such an arrangement did not exhibit any appreciable improvement in power conversion compared to samples with inorganic LPL. The poor performance is attributed to the short-lived charge lifetime, as measured by TRPL. Nevertheless, this study demonstrates a simple strategy for enhancing light absorption by incorporating luminescence compounds into photovoltaic systems, although significant improvement and optimization work are needed, especially for the organic luminescence blend.

Research data policy and data availability statements

Data generated and/or analyzed during the study are available from the corresponding author on reasonable request.

Table 4
I–V performance parameters of perovskite solar cell samples with or without organic LPL, tested under xenon lamp illumination and under dark after light soaking for 5 min.

Samples	Condition	I_{sc} (mA)	V_{oc} (V)	Fill factor	Efficiency (%)
Control	Light	1.78	0.544	25.0	2.21
	Dark	0	0.4	–	–
With strontium-based LPL	Light	5.35	0.512	26.0	6.63
	Dark	0.013	0.228	30.7	1.03
With TMB + PPT blend	Light	2.56	0.285	25.6	1.75
	Dark	0	0.337	25.6	0.08

CRediT authorship contribution statement

Tejas Sharma: Writing – review & editing, Writing – original draft, Methodology, Investigation, Formal analysis. **Thi Thu Ha Nguyen:** Writing – review & editing, Writing – original draft, Investigation, Formal analysis. **Ngoc Ha Nguyen:** Investigation, Formal analysis. **Hoang Lan Ngo:** Investigation, Formal analysis. **Yew Hang Soo:** Methodology. **Chai Yan Ng:** Writing – review & editing. **H. K. Jun:** Writing – review & editing, Writing – original draft, Supervision, Resources, Project administration, Funding acquisition.

Declaration of competing interest

The authors declare the following financial interests/personal relationships which may be considered as potential competing interests:Hieng Kiat Jun reports financial support was provided by the Air Force Office of Scientific Research (AFOSR-AOARD). There is no other conflict of interest to be declared.

Acknowledgements

This material is based upon work supported by the Air Force Office of Scientific Research under award number FA2386-21-1-4106.

References

[1] S. Wu, Z. Pan, R. Chen, X.T.A.-T.T. Liu, Long Afterglow Phosphorescent Materials, Springer Cham, Cham, 2017, https://doi.org/10.1007/978-3-319-60421-3.
[2] Y. Li, M. Gecevicius, J. Qiu, Long persistent phosphors - from fundamentals to applications, Chem. Soc. Rev. 45 (2016) 2090–2136.
[3] L. Ma, Q. Xu, S. Sun, B. Ding, Z. Huang, X. Ma, H. Tian, A universal strategy for tunable persistent luminescent materials via radiative energy transfer, Angew. Chem. Int. Ed. 61 (2022).
[4] Y. Pan, J. Li, X. Wang, Y. Sun, J. Li, B. Wang, K. Zhang, Highly efficient TADF-type organic afterglow of long emission wavelengths, Adv. Funct. Mater. 32 (2022).
[5] Z. Lin, R. Kabe, K. Wang, C. Adachi, Influence of energy gap between charge-transfer and locally excited states on organic long persistence luminescence, Nat. Commun. 11 (2020).
[6] S. Xu, R. Chen, C. Zheng, W. Huang, Excited state modulation for organic afterglow: materials and applications, Adv. Mater. 28 (2016) 9920–9940.
[7] S. Hirata, K. Totani, J. Zhang, T. Yamashita, H. Kaji, S.R. Marder, T. Watanabe, C. Adachi, Efficient persistent room temperature phosphorescence in organic amorphous materials under ambient conditions, Adv. Funct. Mater. 23 (2013) 3386–3397.
[8] T. Wang, M. Liu, J. Mao, Y. Liang, L. Wang, D. Liu, T. Wang, W. Hu, Recent advances in long-persistent luminescence materials based on host–guest architecture, Chin. Chem. Lett. 35 (2024).
[9] G.N. Lewis, D. Lipkin, Reversible photochemical processes in rigid media: the dissociation of organic molecules into radicals and ions, J. Am. Chem. Soc. 64 (1942) 2801–2808.
[10] R. Kabe, C. Adachi, Organic long persistent luminescence, Nature 550 (2017).
[11] R. Rajeswari, N. Islavath, M. Raghavender, L. Giribabu, Recent progress and emerging applications of rare earth doped phosphor materials for dye-sensitized and perovskite solar cells: a review, Chem. Rec. 20 (2020) 65–88.
[12] H. Sun, L. Pan, X. Piao, Z. Sun, Long afterglow SrAl2O4:Eu,Dy phosphors for CdS quantum dot-sensitized solar cells with enhanced photovoltaic performance, J. Mater. Chem. A 1 (2013) 6388–6392.
[13] W.J. Ho, B.J. You, J.J. Liu, W.B. Bai, H.J. Syu, C.F. Lin, Photovoltaic performance enhancement of silicon solar cells based on combined ratios of three species of europium-doped phosphors, Materials 11 (2018).
[14] T.D. Kühne, M. Iannuzzi, M. Del Ben, V.V. Rybkin, P. Seewald, F. Stein, T. Laino, R.Z. Khaliullin, O. Schütt, F. Schiffmann, et al., CP2K: an electronic structure and molecular dynamics software package -Quickstep: efficient and accurate electronic structure calculations, J. Chem. Phys. 152 (2020).
[15] L. Chen, H. Cao, S. Wang, Y. Luo, T. Tao, J. Sun, M. Zhang, Efficient air-stable perovskite solar cells with a (FAI)0.46(MAI)0.40(MABr)0.14(PbI2)0.86(PbBr2)0.14 active layer fabricated: via a vacuum flash-assisted method under RH > 50, RSC Adv. 9 (2019) 10148–10154.
[16] F. Zhang, X. Yang, H. Wang, M. Cheng, J. Zhao, L. Sun, Structure engineering of hole-conductor free perovskite-based solar cells with low-temperature-processed commercial carbon paste as cathode, ACS Appl. Mater. Interfaces 6 (2014) 16140–16146.
[17] J. Yang, M. Fang, Z. Li, Organic luminescent materials: the concentration on aggregates from aggregation-induced emission, Aggregate 1 (2020) 6–18.
[18] Y. Xing, L. Wang, D. Yang, Z. Wang, Z. Hao, C. Sun, B. Xiong, Y. Luo, Y. Han, J. Wang, et al., A novel model on time-resolved photoluminescence measurements of polar InGaN/GaN multi-quantum-well structures, Sci. Rep. 7 (2017).
[19] N. Wu, Y. Wu, D. Walter, H. Shen, T. Duong, D. Grant, C. Barugkin, X. Fu, J. Peng, T. White, et al., Identifying the cause of voltage and fill factor losses in perovskite solar cells by using luminescence measurements, Energy Technol. 5 (2017) 1827–1835.
[20] H. Sun, L. Pan, G. Zhu, X. Piao, L. Zhang, Z. Sun, Long afterglow Sr4Al14O25: Eu, Dy phosphors as both scattering and down converting layer for CdS quantum dot-sensitized solar cells, J. Chem. Soc. Dalton Trans. 43 (2014) 14936–14941.
[21] Y. Deng, S. Lu, Z. Xu, J. Zhang, F. Ma, S. Peng, Enhanced performance of CdS/CdSe quantum dot-sensitized solar cells by long-persistence phosphors structural layer, Sci. China Mater. 63 (2020) 516–523.